PNAS RESEARCH ARTICLE | ENVIRONMENTAL SCIENCES

Global reorganization of atmospheric circulation during Dansgaard–Oeschger cycles

Jens Fohlmeister[a,1,2], Natasha Sekhon[b,c], Andrea Columbu[d], Guido Vettoretti[e], Nils Weitzel[f,g], Kira Rehfeld[f,g,h], Cristina Veiga-Pires[i], Maya Ben-Yami[a,j], Norbert Marwan[a], and Niklas Boers[a,j,k,l]

Edited by Sylvia Dee, Department of Earth, Environmental and Planetary Science, Rice University, Houston, TX; received February 27, 2023; accepted June 26, 2023 by Editorial Board Member Jean Jouzel

Ice core records from Greenland provide evidence for multiple abrupt cold–warm–cold events recurring at millennial time scales during the last glacial interval. Although climate variations resembling Dansgaard–Oeschger (DO) oscillations have been identified in climate archives across the globe, our understanding of the climate and ecosystem impacts of the Greenland warming events in lower latitudes remains incomplete. Here, we investigate the influence of DO-cold-to-warm transitions on the global atmospheric circulation pattern. We comprehensively analyze $\delta^{18}O$ changes during DO transitions in a globally distributed dataset of speleothems and set those in context with simulations of a comprehensive high-resolution climate model featuring internal millennial-scale variations of similar magnitude. Across the globe, speleothem $\delta^{18}O$ signals and model results indicate consistent large-scale changes in precipitation amount, moisture source, or seasonality of precipitation associated with the DO transitions, in agreement with northward shifts of the Hadley circulation. Furthermore, we identify a decreasing trend in the amplitude of DO transitions with increasing distances from the North Atlantic region. This provides quantitative observational evidence for previous suggestions of the North Atlantic region being the focal point for these archetypes of past abrupt climate changes.

glacial climate | stadial-interstadial transitions | speleothem | climate model

Significance

Dansgaard–Oeschger (DO) events are pronounced abrupt climate transitions between so-called stadial and interstadial conditions during glacial intervals. Our study targets a long-standing question in paleoclimatology, concerning the global-scale atmospheric reorganization during these rapid large-scale climate transitions with a comprehensive analysis of globally distributed speleothem proxy data. The global dataset suggests significant large-scale shifts in the atmospheric circulation pattern associated with the DO events. We show that the proxy-inferred changes are consistent with simulations of a state-of-the-art Earth system model and explain the reorganization on that basis.

The last glacial period, which lasted approximately from 120 ka to 15 ka B.P., was punctuated by rapid millennial-scale climate variations that have been termed Dansgaard–Oeschger (DO) cycles. These cycles consist of relatively cold (stadial) and warm (interstadial) phases as well as comparably rapid, decadal-scale transitions between them, and have been observed in many paleoclimate proxy archives such as ice cores from Greenland (1–3) and Antarctica (4, 5), marine records (6–8), loess deposits (9), lake sediments (10, 11), and speleothems (12–14). The core region of these fluctuations is believed to be the North Atlantic (15, 16), where they manifest most prominently as rapid warming events (3). The transition from stadial to interstadial climate conditions is accompanied by a rapid warming with an amplitude of up to 16.5 °C within a few decades over Greenland, as inferred from $\delta^{18}O$ and $\delta^{15}N$ measurements in Greenland ice cores (17). A gradual cooling follows the initial abrupt warming, before an abrupt transition back to stadial conditions occurs. A pronounced reorganization of atmospheric storm tracks is inferred by the Ca^{2+} proxy, which records the amount of dust transported to Greenland (3) and which is strongly reduced during interstadials (Fig. 1). Suggestions of a global-scale atmospheric reorganization have been made on the basis of stable oxygen isotope ratios in speleothems (18–20). Up to now, however, the complex atmospheric circulation shifts during stadial–interstadial transitions have only been reconstructed sporadically and locally from this continental archive (Fig. 1; 12, 13, 19).

The stadial–interstadial transitions are accompanied by large reductions of perennial sea ice cover occurring contemporaneously with the rapid temperature increase over Greenland, as suggested by climate model simulations (16, 25, 26) and reconstructions from marine sediment cores in the Nordic Sea (Fig. 1; (21, 27). The rapid shifts in proxies of Greenland air temperature (represented by $\delta^{18}O$ in ice) and atmospheric circulation (represented by Ca^{2+} concentration in ice), as well as of North Atlantic sea ice cover, have been shown to occur—within age uncertainties—simultaneously with a reorganization of the Atlantic Meridional Overturning Circulation (AMOC), as recorded by Pa/Th of marine sediments and $\delta^{13}C$ of benthic foraminifera from the Bermuda Rise (Fig. 1; 22). During interstadials, a decrease in Pa/Th suggests a stronger AMOC, with a strength similar to Holocene values, while the increase in $\delta^{13}C$ indicates a smaller influence of the glacial equivalent of modern Antarctic Bottom Water (AABW), a result consistent with

Author contributions: J.F. and N.B. designed research; J.F. performed research; J.F., N.S., A.C., N.W., K.R., C.V.-P., M.B.-Y., and N.M. analyzed data; G.V. provided and analysed climate model simulations; and J.F., N.S., A.C., G.V., N.W., K.R., C.V.-P., M.B-Y., N.M., and N.B. wrote the paper.

The authors declare no competing interest.

This article is a PNAS Direct Submission. S.D. is a guest editor invited by the Editorial Board.

[1]Present address: Department of Environmental Radioactivity, German Federal Office for Radiation Protection, 10318 Berlin, Germany.

[2]To whom correspondence may be addressed. Email: jfohlmeister@bfs.de.

This article contains supporting information online at https://www.pnas.org/lookup/suppl/doi:10.1073/pnas.2302283120/-/DCSupplemental.

Published August 28, 2023.

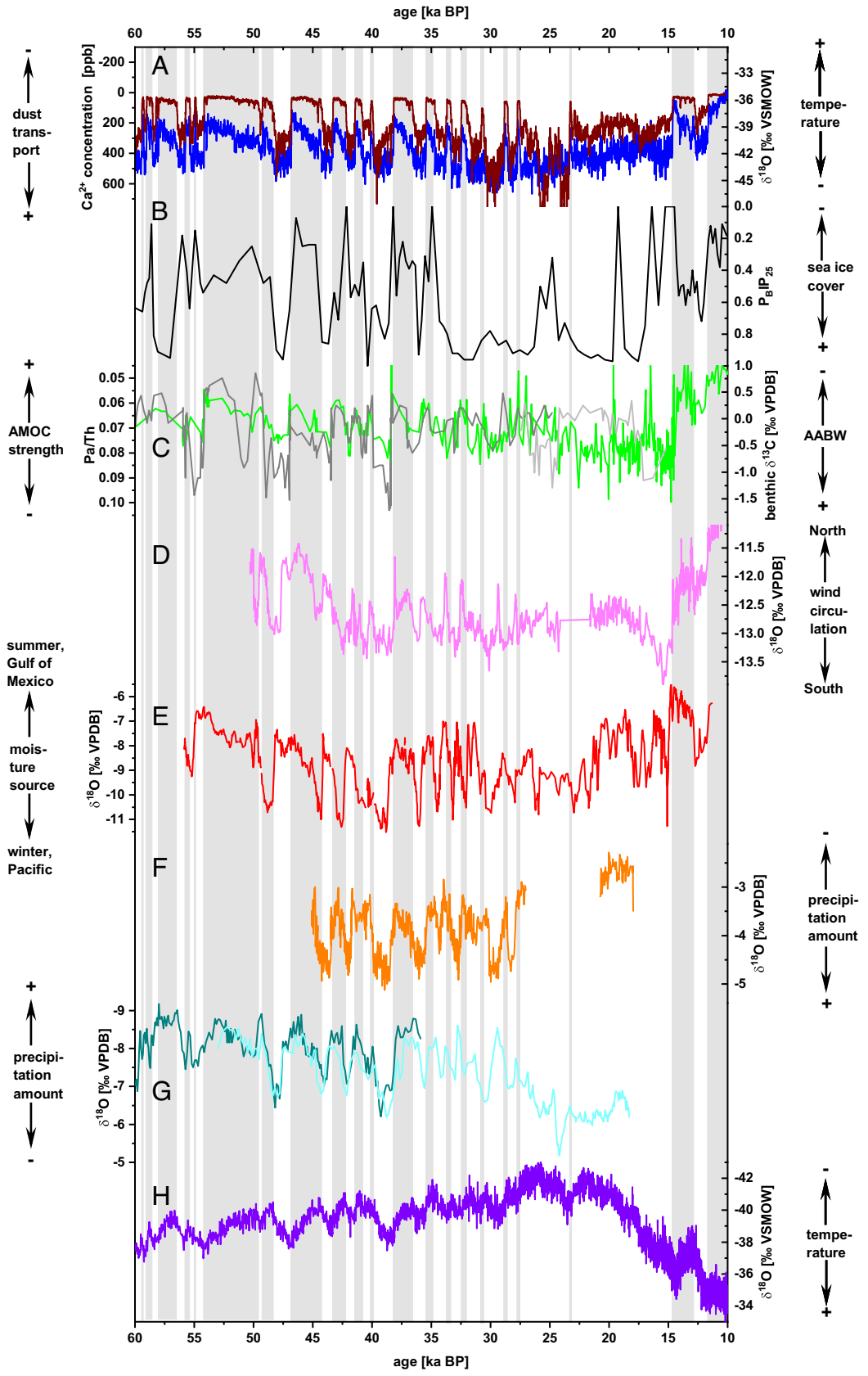

Fig. 1. Climate records of DO cyclicity. Evidence of DO-event is provided from various locations for the period between 60 and 10 ka B.P. (*A*) Greenland stable oxygen isotope (blue) and dust (brown) records (3) are proxies for temperature and atmospheric circulation changes. (*B*) Sea ice cover is provided by the PBIP25 (brassicasterol C25 isoprenoid lipid) sea ice indicator from the SE Norwegian Sea (21). (*C*) The strength of the AMOC (gray) and the influence of AABW (green) at the Bermuda Rise is represented by Pa/Th and δ^{13} C of benthic foraminifera (22, 23). Wind circulation pattern in (*D*) Eastern Europe/western Asia (13) and (*E*) central North America (19) are obtained from δ^{18}O values of speleothem carbonate. Amount of precipitation in (*F*) South America (24) and (*G*) Eastern Asia (5), inferred from δ^{18}O values of speleothem carbonates. (*H*) Antarctic temperature changes (5) from stable isotope composition of ice. Gray bars denote the duration of interstadials as defined from Greenland (3). Locations of records are indicated in Fig. 2.

increased AMOC strength as derived from a fully coupled ocean–atmosphere global climate model (28).

It is believed that the signal of abrupt warming spreads from the North Atlantic region over large parts of the Earth in rapid succession (15, 29). A lag of around 120 y between the warming transitions in Greenland and corresponding temperature maxima in Antarctica has been reported (5, 30), supporting evidence for the interhemispheric redistribution of heat through the ocean by the so-called bipolar seesaw (31, 32). This result suggests a north-to-south directionality, propagated by oceanic processes to the high latitudes of the Southern Hemisphere. In contrast, no significant and systematic leads or lags between the onset of the rapid warming events in Greenland and corresponding transition onsets in independently dated continental archives of the low to mid-latitudes could be found (14, 33, 34), which hints at a rapid transport of the initial climate anomaly from the North Atlantic across the entire northern hemisphere and low latitudes, leading to a reorganization in storm tracks and atmospheric circulation patterns.

Materials and Methods

Here, we focus on the amplitudes of these transitions in atmospheric circulation, investigating their global pattern and spatial distribution, as well as their impact on shifts in moisture source regions, changes in seasonality, and in the amount of precipitation, as recorded in speleothem $\delta^{18}O$ records. We utilize $\delta^{18}O$ records of 111 speleothems from 67 different caves distributed across all continents except Antarctica. The data were extracted from the second version of the Speleothem Isotope Synthesis and Analysis (SISAL) database (35). A detailed description of the data and choice of criteria for suitable speleothems is provided in the supplement. We analyze the time series with respect to abrupt climate warming events–i.e., detection of DO transitions from stadial to interstadial climate conditions. To detect the transitions in the different time series, we follow an established method (9), sliding two neighboring windows through the datasets of $\delta^{18}O$ values. The largest difference of the averaged values in both windows provides an estimate for the center point of a potential abrupt transition. To be assigned as a transition, the strong change in $\delta^{18}O$ must moreover be close to a known stadial–interstadial transition (3; for technical details, see supplement). In our study, we focus on interstadial minus stadial $\delta^{18}O$ differences in precipitation derived from speleothem $\delta^{18}O$ values.

In addition to speleothem $\delta^{18}O$ time series, we analyze the global patterns of temperature and precipitation changes associated with stadial–interstadial transitions that arise naturally and unforced in a fully coupled version of the National Center for Atmospheric Research (NCAR) Community Climate System Model, version 4 (CCSM4; 36, 37). Applied boundary conditions (trace gases, orbital configuration, land-sea mask, and continental ice shields) were those of 21 ka B.P. The model was run at 1° × 1° for both the atmosphere and ocean, a resolution comparable to CMIP5 models (for details, see *SI Appendix*). We calculated 100-y averages of precipitation and temperature data during each stadial and interstadial state and determined the difference in order to compare them to the speleothem $\delta^{18}O$ differences.

Results

Speleothem $\delta^{18}O$ is enriched compared to $\delta^{18}O$ in cave drip water by temperature-dependent fractionation processes during carbonate deposition on speleothem surfaces. Cave air temperature is generally well represented by mean annual air temperatures. Therefore, we can account for this fractionation process by using CCSM4-derived mean annual air temperature for stadials and interstadials and applying a laboratory-based fractionation equation (38). Thus, we can derive the $\delta^{18}O$ values for drip water during stadials and interstadials. Note that the choice of a different temperature–fractionation relationship obtained in other studies (39, 40) does not influence the results as we focus on $\delta^{18}O$ changes instead of absolute temperatures and the temperature–fractionation slope is similar for all relevant studies. The oxygen isotope fractionation within the cave due to temperature changes is mostly small, except for Europe where temperature differences between stadials and interstadials are largest (*SI Appendix*, Fig. S8). Global datasets for $\delta^{18}O$ of precipitation and cave drip water indicate that the mean drip water $\delta^{18}O$ closely represents variations in $\delta^{18}O$ of local precipitation (41) and especially as we investigate climate-driven changes in $\delta^{18}O$ of two climate states, climate-independent cave site-specific offsets will cancel. Hence, drip water $\delta^{18}O$ variations as derived by speleothem $\delta^{18}O$ values can primarily be interpreted as a proxy for $\delta^{18}O$ changes in precipitation, which in turn is often used as a proxy for both precipitation amounts and changes in moisture sources (19, 20), although other less important processes can impact $\delta^{18}O$ at specific locations as well.

We find the $\delta^{18}O$ time series to exhibit characteristic patterns of the stadial–interstadial transitions for each of the 111 speleothems. The range of the $\delta^{18}O$ difference in precipitation for individual stadial–interstadial transitions is approximately between −3.5 and +4.9‰, where a negative sign indicates more negative $\delta^{18}O$ values during interstadials compared to stadials, and a positive sign is related to less negative $\delta^{18}O$ values. We take the median amplitude of these individual transitions over each cave site for a more robust data evaluation, reducing the impact of possible outliers originating from growth rate and data resolution variations. The median stadial–interstadial transition amplitudes range from −3.1 to +2.4‰ during the last glacial period. Compared to the median $\delta^{18}O$ changes of a stadial–interstadial transition in Greenland's NGRIP data (around 3.5‰), the absolute median values of $\delta^{18}O$ changes during stadial–interstadial transitions are smaller for all speleothem records investigated. We observe a pronounced global pattern with spatial heterogeneity of opposite signs in speleothem $\delta^{18}O$ changes (Fig. 2).

Discussion

For Asia, more negative $\delta^{18}O$ values in precipitation during interstadials compared to stadials are observed in the speleothem records (Fig. 2). Following the general interpretation of $\delta^{18}O$ values in paleoclimate data from the South Asian monsoon region (12, 42, 43), namely that decreases of $\delta^{18}O$ reflect more humid trends, the amount of precipitation is higher during interstadials than stadials. This is in line with the interpretation of isotope-enabled GCM data focussing on freshwater-induced millennial-scale cooling events (44, 45) and is consistent with the CCSM4 simulations, where large parts of the southern Asian monsoon region show wetter conditions during interstadials (Fig. 2*A*). We note here that modeling studies focussing on the East Asian Summer Monsoon system highlight an important contribution of the precipitation history (44, 45), but also argue for variations of the precipitation source regions (46) to explain observed shifts in $\delta^{18}O$ in precipitation.

Unfortunately, there is only little information from other speleothem precipitation-sensitive proxies available in this region. Often, the Mg/Ca ratio and Sr/Ca ratio are considered as more reliable proxies to trace changes in the amount of precipitation. To date, the only study focussing on $\delta^{18}O$ and trace elements for millennial-scale variability during the deglacial period indeed suggests that $\delta^{18}O$ records in the northern/eastern Asian monsoon region do not necessarily reflect changes in the amount of precipitation but possibly in the length of the annual monsoon rainfall (47).

Changes in the amount of precipitation also constitute the leading interpretation for variations in $\delta^{18}O$ values in speleothems from the South American monsoon domain (18, 48).

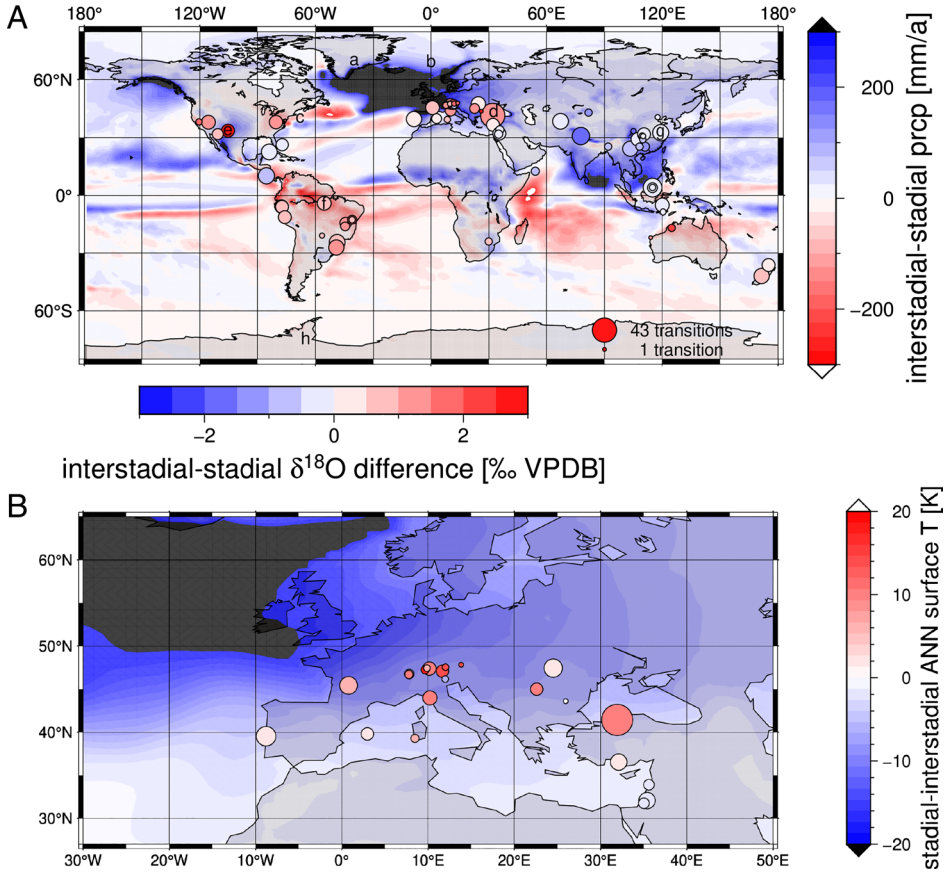

Fig. 2. Stadial–interstadial changes. (*A*) Global map of interstadial–stadial $\delta^{18}O$ difference as recorded in speleothem data (circles, horizontal color bar, median values) during the last glacial. The size of the circles highlights the number of detected events per cave site. Please note that some sites can have more DO events as counted for NGRIP, as several speleothems from one site may exist. In the background interstadial–stadial annual precipitation anomalies are plotted as modeled with the CSSM4 climate model (37); vertical color bar). Letters a to h refer to sites shown in Fig. 1. (*B*) Zoom into Europe for a more detailed view on interstadial–stadial temperature changes. Circles as in (*A*).

However, modeling studies showed that $\delta^{18}O$ changes, especially in eastern Brazil, are also enhanced by a direct propagation of $\delta^{18}O$-depleted meltwater effects (49). During stadial–interstadial transitions, speleothems from South America show an increase in their stable oxygen isotopic composition, representing dryer conditions during interstadials compared to stadials. Thus, the $\delta^{18}O$ values of the stadial–interstadial transitions in this region react in the opposite way compared to the Asian monsoon region, where the $\delta^{18}O$ shifts have been mainly ascribed to a northward shift of the Intertropical Convergence Zone (ITCZ, (18, 48, 50). Such a shift was previously predicted by modeling studies investigating the impact of high-latitude warming and reduced sea ice cover on the position of the ITCZ (51). A northward shift in the mean position of the ITCZ goes in concert with an associated asymmetry in the Hadley circulation in the two hemispheres (18) as well as a northward displacement of the upper-level subtropical westerly jet. Hemispherically averaged, this asymmetry results in more precipitation in the northern hemisphere monsoon regions and less precipitation in the Southern Hemisphere monsoon regions during interstadial conditions (42). A similar feature is also present in the CCSM4 model data. Indeed, the northward-shifted ITCZ during interstadials is expressed by a higher (lower) rainfall amount in the northern (southern) hemispherical (sub) tropical regions (Fig. 2*A*).

Stable oxygen isotope and model results indicate that other regions, such as the subtropical northern hemisphere, are also affected by the shift of the ITCZ and an associated reorganization of the Hadley Circulation. For example, we see a decrease in speleothem $\delta^{18}O$ in the Caribbean (Fig. 2*A*) during stadial–interstadial transitions. This has been reported to reflect an increased amount of rainfall in response to an ITCZ shift toward more northern locations during interstadials (52, 53) and is present in all speleothem records from this region. In contrast, the CCSM4 model results show a heterogeneous precipitation pattern for the Caribbean and do not indicate a clear direction and high level of agreement compared to South and South-East Asia and the northern part of South America.

For all of Europe, we observe a consistent increase in $\delta^{18}O$ values in precipitation during stadial–interstadial transitions (Fig. 2*B*), which most likely has a common cause. One possible process is a change in the $\delta^{18}O$ values and temperature of the moisture source. Stable oxygen isotope values derived from planktonic foraminifera of marine sediments in the Atlantic (Iberian Margin and off Ireland) show differences of about 1‰ with lower values during interstadials (13, 54). At the same time, they show warmer surface waters by about 10 °C. A 10 °C change of surface water (8, 55, 56) indicates that seawater $\delta^{18}O$ values must have been about 1.2‰ higher in interstadials compared to stadials using commonly accepted oxygen isotope fractionation factors (38–40). This value is comparable to the observed averaged interstadial–stadial $\delta^{18}O$ differences in precipitation at European cave sites (0.95‰). We conclude that $\delta^{18}O$ changes at the moisture source seem to be the main reason to explain most of the observed $\delta^{18}O$ differences during stadial–interstadial transitions over the European continent.

Another cluster of speleothem records located over North America also shows an increase in $\delta^{18}O$ values during stadial–interstadial transitions. This region is situated well within the present-day westerly wind system. The stadial–interstadial shifts in speleothem $\delta^{18}O$ from the North American continent have originally been interpreted in terms of northward shifts in the westerly storm tracks (Fort Stanton Cave; 19) and related to changes in seasonal precipitation, with summers usually showing higher $\delta^{18}O$ values compared to winters. The other speleothems from the North American continent show a consistent pattern compared to Fort Stanton speleothems and thus highlight the general applicability of this interpretation. The change in precipitation seasonality is also present in the model data, which show either a strong increase in summer precipitation (Midwest United States) or a reduction of winter rainfall (Western United States) for interstadial compared to stadial conditions (*SI Appendix*, Fig. S9). An updated explanation is provided by a recent proxy data–climate model comparison study (57). This study suggests tropical–extratropical teleconnections for observed $\delta^{18}O$ changes as the driving mechanism for increased winter moisture supply from subtropical latitudes during stadial periods in the Western United States. This explanation again stresses the importance of precipitation seasonality.

There is relatively less data available from the Southern Hemisphere outside the tropics. Nevertheless, the negative values observed from the two cave sites in New Zealand (Fig. 2*A*) suggest a northward shift in the westerly wind system of the Southern Hemisphere during interstadials, which occur in concert with the derived northern hemisphere westerly and ITCZ shifts. This shift in the westerlies most likely led to a change in the source of precipitation.

Recently, there was a model setup published, which was designed to model the stable oxygen isotope composition of precipitation during the last deglaciation (isotope-enabled transient climate experiment—iTraCE, (45, 58) with different forcing (greenhouse gases, ice sheet topographies, orbital parameters, injection of freshwater). When considering the transition from the Heinrich 1 state to the Bølling/Allerød phase during the last deglaciation and using the fully forced experiment setup (greenhouse gases, orbital forcing, freshwater, and ice sheets) as an equivalent for the glacial stadial–interstadial transitions, it might be suitable to compare the speleothem data with the iTraCE results. Overall, there is excellent agreement between the speleothem-derived interstadial–stadial $\delta^{18}O$ offsets in precipitation and the results for the stable oxygen composition of precipitation of the iTraCE model experiments (*SI Appendix*, Fig. S6 and section 5). This comparison, using an additional, independent model simulation, strongly corroborates our results presented in Fig. 2*A*.

We proceed with analyzing the cave-site-specific mean interstadial–stadial differences in $\delta^{18}O$ with respect to latitude (Fig. 3). The northern hemisphere high to midlatitudes show strong positive values. Toward lower latitudes, the offset becomes less positive and turns into a negative shift until a minimum is reached in the latitudinal belt between 20°N and 40°N. The more southward isotope shift for the North American sites compared to the ones in Europe and Asia might likely be explained by the more southward extent of the Laurentide ice sheet as compared with the Fennoscandian one. From about 20°N toward the equator and further south (10°S to 30°S), the $\delta^{18}O$ differences for stadial–interstadial transitions increase. In general, the absolute values of the data between 10°S to 30°S are smaller than those in the northern hemisphere mid-latitudes, albeit some large interstadial–stadial differences are observable on the South American continent. The values even further south than 30°S show less positive interstadial–stadial $\delta^{18}O$ differences again. In the Southern Hemisphere, only a few cave sites are available and the robustness of those

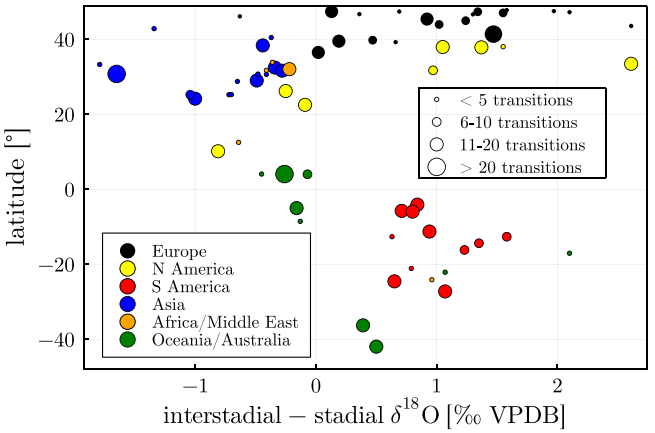

Fig. 3. Latitudinal distribution of interstadial–stadial differences in $\delta^{18}O$ in precipitation. Results from all individual stadial–interstadial transitions (*SI Appendix*, Fig. S10) shown as median for individual cave sites. The color code of data points reflects the location of the sites, while the size of the data point visualizes the number of detected transitions. A S-like shape is observed, where the bow in the Southern Hemisphere shows smaller interstadial–stadial differences than its counterpart in the northern hemisphere.

observations could be questioned, but the described features appear also to be valid, when accounting for all detected individual events (*SI Appendix*, Fig. S10).

Outside of Europe, where strong moisture source temperature and $\delta^{18}O$ changes superimpose the precipitation $\delta^{18}O$ changes, the $\delta^{18}O$ pattern in precipitation is consistent with the above-discussed changes in global atmospheric circulation patterns. During a stadial–interstadial transition, the mean ITCZ position is shifted northward, resulting in decreased precipitation in South America, while at the same time the northward ITCZ shift results in lower $\delta^{18}O$ values in the monsoon regions of the northern hemisphere — e.g., in the Caribbean, on the Indian subcontinent, and over large parts of China. At the same time, the northward ITCZ shift during the phases of strong sea ice reduction is accompanied by a northward shift of the westerlies, which contributes to the observed changes in $\delta^{18}O$ over North America and New Zealand.

To further investigate the geographical origin of stadial–interstadial transitions, we consider the change of the absolute amplitude of interstadial–stadial $\delta^{18}O$ differences with increasing distance from the North Atlantic region. Our analysis shows that among all records, the largest speleothem $\delta^{18}O$ interstadial–stadial differences are from caves closest to this region (Fig. 4).

As some caves and speleothems might not detect the full $\delta^{18}O$ amplitude of stadial–interstadial transitions (*SI Appendix*, section 6), we consider only the amplitude for those cave sites that represent the largest 33% of all values per 2,500 km distance bin in the following. The mean $\delta^{18}O$ difference of the speleothems within the group of the maximum amplitude sites for a given distance decreases with increasing distance from the high northern latitudes (Fig. 4). This is a robust feature, independent of the applied cut-off value (*SI Appendix*, *supplemental text* and Fig. S7) and with a correlation coefficient between the considered $\delta^{18}O$ differences and distance from Greenland of −0.62 ($p < 0.01$). Modeled relative absolute precipitation changes between interstadials and stadials at the cave sites show a similar behavior. This proxy data- and model-based observation provides additional information on the geographical origin of the DO events. From a potential source region where the transitions are triggered, any signal is expected to attenuate with increasing distance from that origin. We hypothesize that this is also a valid feature in the complex and highly nonlinear climate system, because for longer distances, the influence of other processes modifying the

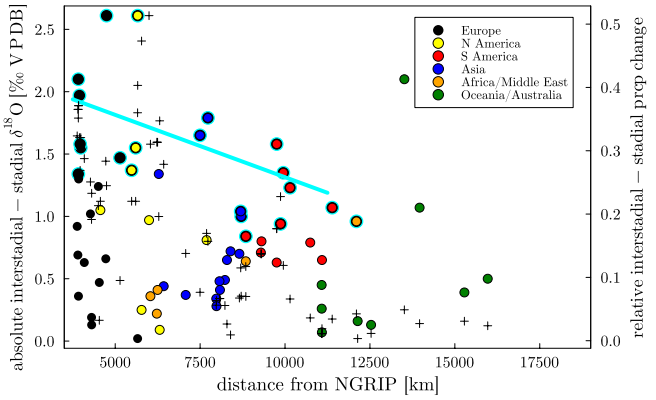

Fig. 4. Change in the absolute amplitude of interstadial–stadial $\delta^{18}O$ differences in precipitation (circles, left *y* axis, median values) and CCSM4-based relative absolute precipitation changes at the cave sites (crosses, right *y* axis) with respect to their distance from the North Atlantic region, i.e., the location of NGRIP. A decreasing trend of the 33% of the largest $\delta^{18}O$ transitions per 2,500 km bin (cyan marker stroke color and according cyan colored trendline with y = −0.0001 x +2.3142 and r = −0.62, p < 0.01) is observed, highlighting an attenuation of the climate effect of stadial–interstadial transitions with increasing distance to the North Atlantic, which is also supported by the climate model. The bins beyond 12,500 km distance were not used, due to the small number of cave sites.

signal will increase. We hence present empirical evidence that the origin of DO events can be traced back to the northern high latitudes.

A similar feature is also present for the Heinrich 1—Bølling/Allerød transition in the iTraCE experiment. The $\delta^{18}O$ differences in precipitation between the warm Bølling/Allerød and the preceding cold Heinrich 1 event show a similar decreasing $\delta^{18}O$ difference with increasing distance from the North Atlantic core region (*SI Appendix*, Fig. S7) providing support for our speleothem-derived observation. It is expected that the direct response in the mid-latitudes of the northern hemisphere is larger than the response in the Southern Hemisphere because of atmospheric wave propagation. This could explain why there exist some regions closer to the North Atlantic core region in both simulation products (e.g., the Mediterranean sites), which show a smaller response than some locations farther away (e.g., southern American sites). Nevertheless, the statistically highly significant relationship between signal and distance from the North Atlantic core region suggests the existence of a general physical mechanism responsible for the signal attenuation despite deviations from the overall trend due to local characteristics. We propose that the signal attenuation is driven by temperature and temperature gradient changes during stadial–interstadial transitions being largest close to the North Atlantic. As relevant variables for precipitation and its isotopic signature such as sea level pressure, evaporation, and winds are strongly influenced by the temperature and temperature gradient changes (59, 60), the signal attenuation could be imprinted onto precipitation and its oxygen isotope signature. This would lead to these two variables showing a similar signal attenuation structure as temperatures. However, the exact processes have yet to be investigated.

We have thus provided a consistent global analysis of stadial–interstadial transitions with a focus on associated changes in atmospheric circulation and precipitation. The maximum amplitudes support the hypothesis that the North Atlantic region is the trigger of the stadial–interstadial transitions. We were able to obtain a global picture of changes in $\delta^{18}O$ of precipitation related to stadial–interstadial transitions, which helps to define the geographical constraints on the maximum shifts of the mean position of the ITCZ and an associated relocation in the mid-latitude westerlies. Our proxy-based findings are in remarkable agreement with simulations of unforced DO-type oscillations with a state-of-the-art, high-resolution climate model and simulated oxygen isotope changes in a fully forced transition between Heinrich stadial 1 and the Bølling/Allerød phase. Our results will be used as benchmarks for other isotope-enabled general circulation models to investigate the stadial–interstadial transitions in future research, aiming for a more complete picture of abrupt climate changes in comprehensive climate models.

Data, Materials, and Software Availability. SISAL data are available at https://researchdata.reading.ac.uk/256/ (61). The code for data extraction and numerical analysis is available at https://github.com/jensfohlmeister/Sisal_DO_analysis (62). Previously published data were used for this work (35, 37).

ACKNOWLEDGMENTS. This is TiPES (Tipping Points in the Earth System) contribution #103; the TiPES project has received funding from the European Union's Horizon 2020 research and innovation program under grant agreement No. 820970. N.B. acknowledges further funding by the Volkswagen Foundation. M.B.-Y. and N.B. acknowledge additional funding by the European Union's Horizon 2020 research and innovation programme under the Marie Sklodowska–Curie grant agreement No. 956170. C.V.-P. acknowledges the financial support of the Portuguese Foundation of Science and Technology to Centre for Marine and Environmental Research through UID/00350/2020 CIMA. N.W. and K.R. acknowledge funding by the Deutsche Forschungsgemeinschaft project no. 395588486 and the German federal ministry of Education and Research through the Palmod project (code 01LP1926C). This study includes data compiled by SISAL, a working group of the Past Global Changes (PAGES) project and is in part inspired by discussions at a SISAL workshop in Xi'an (China) in 2019. PAGES received support from the Swiss Academy of Sciences and the Chinese Academy of Sciences.

Author affiliations: [a]Potsdam Institute for Climate Impact Research, 14473 Potsdam, Germany; [b]Department of Earth, Environmental, and Planetary Sciences, Brown University, Providence, RI 02912; [c]Institute at Brown for Environment and Society, Brown University, Providence, RI 02912; [d]Department of Earth Sciences, University of Pisa, 56126 Pisa, Italy; [e]Physics of Ice, Climate and Earth, Niels Bohr Institute, University of Copenhagen, 2200 Copenhagen, Denmark; [f]Department of Geosciences, University of Tübingen, 72076 Tübingen, Germany; [g]Institute of Environmental Physics, Heidelberg University, 69120 Heidelberg, Germany; [h]Department of Physics, University of Tübingen, 72076 Tübingen, Germany; [i]Centre for Marine and Environmental Research, Faculty of Sciences and Technology, Universidade do Algarve, Campus de Gambelas, 8005-139 Faro, Portugal; [j]Earth System Modelling, School of Engineering & Design, Technical University of Munich, Munich 80333, Germany; [k]Global Systems Institute, University of Exeter, Exeter EX4 4QF, UK; and [l]Department of Mathematics, University of Exeter, Exeter EX4 4QF, UK

1. W. Dansgaard *et al.*, Evidence for general instability of past climate from a 250-kyr ice-core record. *Nature* **364**, 218–220 (1993).
2. North Greenland Ice Core Project members, High-resolution record of the Northern Hemisphere climate extending into the last interglacial period. *Nature* **431**, 147–151 (2004).
3. S. O. Rasmussen *et al.*, A stratigraphic framework for abrupt climatic changes during the Last Glacial period based on three synchronized Greenland ice-core records: refining and extending the INTIMATE event stratigraphy. *Quat. Sci. Rev.* **106**, 14–28 (2014).
4. T. Blunier, E. J. Brook, Timing of millennial-scale climate change in Antarctica and Greenland during the last glacial period. *Science* **291**, 109–112 (2001).
5. C. Buizert *et al.*, Precise interpolar phasing of abrupt climate change during the last ice age. *Nature* **520**, 661–665 (2015).
6. G. Bond *et al.*, Correlations between climate records from North Atlantic sediments and Greenland ice. *Nature* **365**, 143 (1993).
7. J. F. McManus, D. W. Oppo, J. L. Cullen, A 0.5-million-year record of millennial-scale climate variability in the North Atlantic. *Science* **283**, 971–975 (1999).
8. B. Martrat *et al.*, Four climate cycles of recurring deep and surface water destabilizations on the Iberian margin. *Science* **317**, 502–507 (2007).
9. D. D. Rousseau *et al.*, (MIS3 & 2) millennial oscillations in Greenland dust and Eurasian aeolian records–A paleosol perspective. *Quat. Sci. Rev.* **169**, 99–113 (2017).
10. J. R. Allen *et al.*, Rapid environmental changes in southern Europe during the last glacial period. *Nature* **400**, 740–743 (1999).
11. P. C. Tzedakis, H. Hooghiemstra, H. Pälike, The last 1.35 million years at Tenaghi Philippon: Revised chronostratigraphy and long-term vegetation trends. *Quat. Sci. Rev.* **25**, 3416–3430 (2006).
12. Y. J. Wang *et al.*, A high-resolution absolute-dated late Pleistocene monsoon record from Hulu Cave, China. *Science* **294**, 2345–2348 (2001).

13. D. Fleitmann *et al.*, Timing and climatic impact of Greenland interstadials recorded in stalagmites from northern Turkey. *Geophys. Res. Lett.* **36**, L19707 (2009).
14. G. E. Moseley *et al.*, NALPS19: Sub-orbital-scale climate variability recorded in northern Alpine speleothems during the last glacial period. *Clim. Past* **16**, 29–50 (2020).
15. A. Ganopolski, S. Rahmstorf, Rapid changes of glacial climate simulated in a coupled climate model. *Nature* **409**, 153–158 (2001).
16. L. C. Sime, P. O. Hopcroft, R. H. Rhodes, Impact of abrupt sea ice loss on Greenland water isotopes during the last glacial period. *Proc. Natl. Acad. Sci. U.S.A.* **116**, 4099–4104 (2019).
17. P. Kindler *et al.*, Temperature reconstruction from 10 to 120 kyr b2k from the NGRIP ice core. *Clim. Past* **10**, 887–902 (2014).
18. X. Wang *et al.*, Interhemispheric anti-phasing of rainfall during the last glacial period. *Quat. Sci. Rev.* **25**, 3391–3403 (2006).
19. Y. Asmerom, V. J., Polyak, S. J., Burns, Variable winter moisture in the southwestern United States linked to rapid glacial climate shifts. *Nat. Geosci.* **3**, 114–117 (2010).
20. H. Cheng *et al.*, The Asian monsoon over the past 640,000 years and ice age terminations. *Nature* **534**, 640–646 (2016).
21. U. Hoff, T. L. Rasmussen, R. Stein, M. M. Ezat, K. Fahl, Sea ice and millennial-scale climate variability in the Nordic seas 90 kyr ago to present. *Nat. Commun.* **7**, 1–10 (2016).
22. L. G. Henry *et al.*, North Atlantic ocean circulation and abrupt climate change during the last glaciation. *Science* **353**, 470–474 (2016).
23. J. Lippold *et al.*, Does sedimentary 231Pa/230Th from the Bermuda Rise monitor past Atlantic meridional overturning circulation? *Geophys. Res. Lett.* **36**, L12601 (2009).
24. X. Wang *et al.*, Hydroclimate changes across the Amazon lowlands over the past 45,000 years. *Nature* **541**, 204–207 (2017).
25. C. Li, D. S. Battisti, C. M. Bitz, Can North Atlantic sea ice anomalies account for Dansgaard-Oeschger climate signals? *J. Clim.* **23**, 5457–5475 (2010).
26. N. Boers, M. Ghil, D. D. Rousseau, Ocean circulation, ice shelf, and sea ice interactions explain Dansgaard-Oeschger cycles. *Proc. Natl. Acad. Sci. U.S.A.* **115**, E11005–E11014 (2018).
27. T. M. Dokken, K. H. Nisancioglu, C. Li, D. S. Battisti, C. Kissel, Dansgaard-Oeschger cycles: Interactions between ocean and sea ice intrinsic to the Nordic seas. *Paleoceanography* **28**, 491–502 (2013).
28. J. Lynch-Stieglitz *et al.*, Muted change in Atlantic overturning circulation over some glacial-aged Heinrich events. *Nat. Geosci.* **7**, 144–150 (2014).
29. G. E. Birchfield, W. S. Broecker, A salt oscillator in the glacial Atlantic? Part II A "scale analysis" model. *Paleoceanography* **5**, 835–843 (1990).
30. A. Svensson *et al.*, Bipolar volcanic synchronization of abrupt climate change in Greenland and Antarctic ice cores during the last glacial period. *Clim. Past* **16**, 1565–1580 (2020).
31. T. J. Crowley, North Atlantic Deep Water cools the southern hemisphere. *Paleoceanography* **7**, 489–497 (1992).
32. T. F. Stocker, S. J. Johnsen, A minimum thermodynamic model for the bipolar seesaw. *Paleoceanography* **18**, 1087 (2003).
33. F. Adolphi *et al.*, Connecting the Greenland ice-core and U/Th timescales via cosmogenic radionuclides: Testing the synchroneity of Dansgaard-Oeschger events. *Clim. Past* **14**, 1755–1781 (2018).
34. E. C. Corrick *et al.*, Synchronous timing of abrupt climate changes during the last glacial period. *Science* **369**, 963–969 (2020).
35. L. Comas-Bru *et al.*, SISALv2: A comprehensive speleothem isotope database with multiple age–depth models. *Earth Syst. Sci. Data* **12**, 2579–2606 (2020).
36. W. R. Peltier, G. Vettoretti, Dansgaard-Oeschger oscillations predicted in a comprehensive model of glacial climate: A "kicked" salt oscillator in the Atlantic. *Geophys. Res. Lett.* **41**, 7306–7313 (2014).
37. G. Vettoretti, W. R. Peltier, Fast physics and slow physics in the nonlinear Dansgaard-Oeschger relaxation oscillation. *J. Clim.* **31**, 3423–3449 (2018).
38. S. T. Kim, J. R. O'Neil, Equilibrium and nonequilibrium oxygen isotope effects in synthetic carbonates. *Geochim. Cosmochim. Acta* **61**, 3461–3475 (1997).
39. M. Daëron *et al.*, Most Earth-surface calcites precipitate out of isotopic equilibrium. *Nat. Commun.* **10**, 429 (2019).
40. D. M. Tremaine, P. N. Froelich, Y. Wang, Speleothem calcite farmed in situ: Modern calibration of δ18O and δ13C paleoclimate proxies in a continuously-monitored natural cave system. *Geochim. Cosmochim. Acta* **75**, 4929–4950 (2011).
41. A. Baker *et al.*, Global analysis reveals climatic controls on the oxygen isotope composition of cave drip water. *Nat. Commun.* **10**, 2984 (2019).
42. G. Kathayat *et al.*, Indian monsoon variability on millennial-orbital timescales. *Sci. Rep.* **6**, 24374 (2016).
43. G. Liu *et al.*, On the glacial-interglacial variability of the Asian monsoon in speleothem δ18O records. *Sci. Adv.* **6**, eaay8189 (2020).
44. F. S. Pausata, D. S. Battisti, K. H. Nisancioglu, C. M. Bitz, Chinese stalagmite δ18O controlled by changes in the Indian monsoon during a simulated Heinrich event. *Nat. Geosci.* **4**, 474–480 (2011).
45. C. He *et al.*, Hydroclimate footprint of pan-Asian monsoon water isotope during the last deglaciation. *Sci. Adv.* **7**, eabe2611 (2021).
46. C. R. Tabor *et al.*, Interpreting precession-driven δ18O variability in the South Asian monsoon region. *J. Geophys. Res. Atmos.* **123**, 5927–5946 (2018).
47. H. Zhang *et al.*, East Asian hydroclimate modulated by the position of the westerlies during Termination I. *Science* **362**, 580–583 (2018).
48. H. Cheng *et al.*, Climate change patterns in Amazonia and biodiversity. *Nat. Commun.* **4**, 1411 (2013).
49. J. Zhu *et al.*, Investigating the direct meltwater effect in terrestrial oxygen-isotope paleoclimate records using an isotope-enabled Earth system model. *Geophys. Res. Lett.* **44**, 12–501 (2017).
50. L. C. Kanner, S. J. Burns, H. Cheng, R. L. Edwards, High-latitude forcing of the South American summer monsoon during the last glacial. *Science* **335**, 570–573 (2012).
51. J. C. Chiang, C. M. Bitz, Influence of high latitude ice cover on the marine intertropical convergence zone. *Clim. Dyn.* **25**, 477–496 (2005).
52. M. M. Arienzo *et al.*, Bahamian speleothem reveals temperature decrease associated with Heinrich stadials. *Earth Planet. Sci. Lett.* **430**, 377–386 (2015).
53. S. W. Warken *et al.*, Caribbean hydroclimate and vegetation history across the last glacial period. *Quat. Sci. Rev.* **218**, 75–90 (2019).
54. V. Margari *et al.*, The nature of millennial-scale climate variability during the past two glacial periods. *Nat. Geosci.* **3**, 127–131 (2010).
55. M. J. Vautravers, N. I. Shackleton, Centennial-scale surface hydrology off Portugal during marine isotope stage 3: Insights from planktonic foraminiferal fauna variability. *Paleoceanography* **21**, PA3004 (2006).
56. E. Salgueiro *et al.*, Temperature and productivity changes off the western Iberian margin during the last 150 ky. *Quat. Sci. Rev.* **29**, 680–695 (2010).
57. D. McGee, E. Moreno-Chamarro, J. Marshall, E. D. Galbraith, Western US lake expansions during Heinrich stadials linked to Pacific Hadley circulation. *Sci. Adv.* **4**, eaav0118 (2018).
58. C. He *et al.*, Abrupt Heinrich Stadial 1 cooling missing in Greenland oxygen isotopes. *Sci. Adv.* **7**, eabh1007 (2021).
59. M. P. Byrne, P. A. O'Gorman, The response of precipitation minus evapotranspiration to climate warming: Why the "Wet-Get-Wetter, Dry-Get-Drier" scaling does not hold over land. *J. Clim.* **28**, 8078–8092 (2015).
60. W. H. G. Roberts, P. O. Hopcroft, Controls on the tropical response to abrupt climate changes. *Geophys. Res. Lett.* **47**, e2020GL087518 (2020).
61. L. Comas-Bru *et al.*, SISAL (Speleothem Isotopes Synthesis and AnaLysis Working Group) database version 2.0. University of Reading. *Dataset*. https://doi.org/10.17864/1947. 256. Accessed 20 April 2020.
62. J. Fohlmeister, Code for DO analysis of SISAL data. Github. https://github.com/jensfohlmeister/Sisal_DO_analysis. Deposited 10 July 2023.